Study of differential cross-polarization modulation in a semiconductor optical amplifier

Chia Chien Wei and Jason (Jyehong) Chen

Institute of Electro-Optical Engineering and Department of Photonics, National Chiao-Tung University, 1001 Ta Hsueh Rd., Hsin-Chu, Taiwan, 300

mgyso.eo91g@nctu.edu.tw, jchen@mail.nctu.edu.tw

Abstract: Differential cross-polarization modulation (DXPoM) wavelength conversion using a semiconductor optical amplifier has been proposed to outperform substantially traditional cross-polarization modulation (XPoM). This work presents analytical small-signal models of XPoM and DXPoM. The transfer function of DXPoM is used to elucidate the significant improvement in bandwidth and the relationships among the modulation bandwidth, the delay, the operating points and other device parameters of a semiconductor optical amplifier (SOA).

OCIS codes: (190.2620) Frequency conversion; (250.5980) Semiconductor optical amplifiers; (260.1440) Birefringence

References and links

1. S. J. B. Yoo, "Wavelength conversion technologies for WDM network applications," J. Lightwave Technol. **14**, 955-966 (1996).
2. T. Durhuus, B. Mikkelsen, C. Joergensen, S. L. Danielsen, and K. E. Stubkjaer, "All-optical wavelength conversion by semiconductor optical amplifiers," J. Lightwave Technol. **14**, 942-954 (1996).
3. Y. Liu, M. T. Hill, E. Tangdiongga, H. de Waardt, N. Galabretta, G. D. Khoe, and H. J. S. Dorren, "Wavelength conversion using nonlinear polarization rotation in a single semiconductor optical amplifier," IEEE Photonics Technol. Lett. **15**, 90-92 (2003).
4. S. Diez, C. Schmidt, R. Ludwig, H. G. Weber, K. Obermann, S. Kindt, I. Koltchanov, and K. Petermann, "Four-wave mixing in semiconductor optical amplifiers for frequency conversion and fast optical switching," IEEE J. Sel. Top. Quantum Electron. **3**, 1131-1145 (1997).
5. Y. Ueno, S. Nakamura, K. Tajima, and S. Kitamura, "3.8-THz wavelength conversion of picosecond pulses using a semiconductor delay-interference signal-wavelength converter (DISC)," IEEE Photonics Technol. Lett. **10**, 346-348 (1998).
6. J. Leuthold, B. Mikkelsen, R. E. Behringer, G. Raybon, C. H. Joyner, and P. A. Besse, "Novel 3R regenerator based on semiconductor optical amplifier delay-interference configuration," IEEE Photonics Technol. Lett. **13**, 860-862 (2001).
7. B. Mikkelsen, K. S. Jepsen, M. Vaa, H. N. Poulsen, K. E. Stubkjaer, R. Hess, M. Duelk, W. Vogt, E. Gamper, E. Gini, P. A. Besse, H. Melchior, S. Bouchoule and F. Devaux, "All-optical wavelength converter scheme for high speed RZ signal formats," Electron. Lett. **33**, 2137-2139 (1997).
8. S. Nakamura, and K. Tajima, "Bit-rate-transparent non-return-to-zero all-optical wavelength conversion at up to 42 Gb/s by operating Symmetric-Mach-Zehnder switch with new scheme," *OFC'04*, paper FD3, 2004.
9. C. C. Wei, M. F. Huang and J. Chen, "Enhancing the frequency response of cross-polarization wavelength conversion," IEEE Photonics Tenhnol. Lett. **17**, 1683-1685 (2005).
10. D. Marcenac and A. Mecozzi, "Switches and frequency converters based on cross-gain modulation in semiconductor optical amplifiers," IEEE Photonics Tech. Lett. **9**, 749-751 (1997).
11. H. J. S. Dorren, D. Lenstra, Y. Liu, M. T. Hill and G. D. Khoe, "Nonlinear polarization rotation in semiconductor optical amplifiers: theory and application to all-optical flip-flop memories," IEEE J. Quantum Electron. **39**, 141-148 (2003).
12. G. Lenz, B. J. Eggleton, C. R. Giles, C. K. Madsen and R. E. Slusher, "Dispersive properties of optical filters for WDM systems," IEEE J. Quantum Electron. **34**, 1390-1402 (1998).

#8154 - $15.00 USD Received 18 July 2005; Revised 27 September 2005; Accepted 2 October 2005

1. Introduction

All optical wavelength conversion (AOWC) is considered to be an indispensable function in next-generation wavelength routing network architecture [1]. AOWCs based on semiconductor optical amplifiers (SOAs) are particularly attractive because they provide the advantage of monolithic integration and the potential of low-cost production. Various SOA-based AOWCs have been proposed, such as cross-gain modulation (XGM) [2], cross-phase modulation (XPM) [2], cross-polarization modulation (XPoM) [3], four-wave mixing (FWM) [4] and delay-interference signal-wavelength converter (DISC) [5,6]. Based on an interferometric principle that is similar to that exploited by the Mach-Zehnder interferometer (MZI), the XPoM employs the phase difference between the TE and the TM modes as an optical beam passes through an SOA. Accordingly, an additional delay line in the MZI-based XPM [7,8] also works in the XPoM scheme. Restated, simply adding an extra birefringence delay line to the standard XPoM considerably improves the conversion performance. This novel scheme is called differential cross-polarization modulation (DXPoM) [9]. Although the architecture of DXPoM is similar to that of DISC, DXPoM utilizes the interference between two distinct and orthogonal modes achieving wavelength conversion even without an extra delay line. However, DISC employs self-interference, and works only for the RZ format.

Although large-signal simulations have already established the difference between the performance of XPoM and that of DXPoM, and yielded results that agree with the experimental results [9], this study presents the analytical small-signal model to explain the significant performance improvement offered by DXPoM, and to clarify the relationships among modulation bandwidth, the delay, the operating points and other device parameters of an SOA. Furthermore, the optimum delay which corresponds to not only a largest conversion bandwidth but also a least phase distortion is derived analytically from the small-signal model.

2. Implementing DXPoM

Figure 1 presents the configuration of DXPoM. A signal pump laser beam at wavelength λ_1 and a CW probe laser beam at wavelength λ_2 are fed into an SOA, as in a typical XPoM. Properly controlling the polarization states of λ_1 and λ_2 allows the injected pump light to introduce additional birefringence in the SOA, resulting in a change in the difference between the refractive indices of the TE and TM modes of the probe beam. At the polarizer, these two orthogonal modes are partially combined coherently. Restated, the XPoM exploits the phase difference between the TE and TM modes, when the probe beam passes through an SOA, to rotate the polarization state. This phase difference, controlled by the signal power, determines the output power of the CW beam after it has passed through a polarizer. However, an extra birefringence delay line is added in front of the polarizer in the DXPoM to improve the conversion speed of the traditional XPoM.

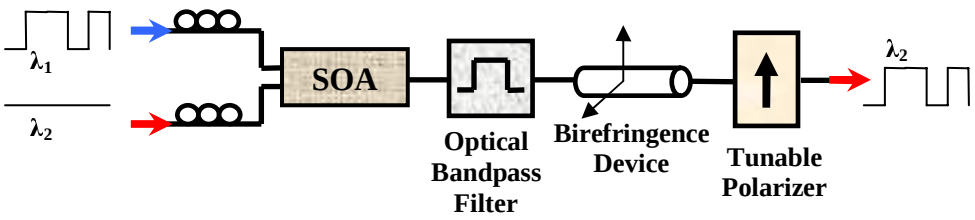

Fig. 1. Configuration of a DXPoM wavelength converter

#8154 - $15.00 USD Received 18 July 2005; Revised 27 September 2005; Accepted 2 October 2005

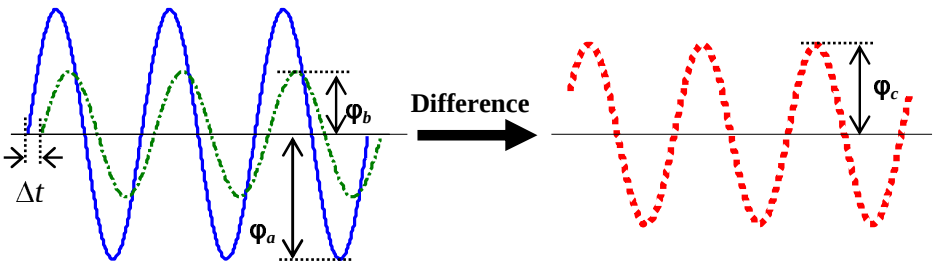

Fig. 2. Illustration of a differential sinusoidal wave

A simplified and intuitive example helps to explain why this extra delay line improves the conversion speed. Figure 2 shows two sinusoidal waves with the same angular frequency, Ω, but different amplitudes, φ_a and φ_b. The difference between these two waves is also a sinusoidal wave with frequency, Ω, and amplitude, φ_c. If the time offset, Δt, as presented in Fig. 2 is applied, then $\varphi_c^2 = \varphi_a^2 + \varphi_b^2 - 2\varphi_a\varphi_b \cos(\Omega\Delta t)$. For $\Omega \leq \pi/\Delta t$, the differential amplitude increases with frequency. Namely, properly selecting Δt increases the differential amplitudes at some frequencies. Accordingly, adding an extra delay between the TE and TM modes may amplify some high-frequency components of the phase difference in DXPoM, to compensate for the insufficient frequency response associated with the long lifetime of the carriers in an SOA. The polarization state of the output CW beam after the delay line is passed is rotated more rapidly as the signal power varies. Consequently, DXPoM has a higher conversion speed and a better performance than XPoM.

3. Small-signal models of XPoM

Based on the equations derived in references [10,11], the propagating equations of the optical fields in an SOA are,

$$\frac{d\wp_i^k}{dz} = \left[\Gamma^k a_i^k \left(\eta^k N - N_i\right) - \alpha_{loss}^k\right]\wp_i^k, \qquad k = TE, TM \tag{1}$$

$$\frac{dN}{dt} = -\frac{N}{\tau_s} - \sum_{i,k}\left[a_i^k \left(\eta^k N - N_i\right)\frac{\wp_i^k}{\hbar\omega_i A_{eff}}\right] + \frac{I}{eV} \tag{2}$$

where i =1, 2 represent the signal and the CW beam, respectively. ω_i and N_i are the optical angular frequency and the carrier density at transparency of the i beam; $\wp_i^k$ and a_i^k are the optical intensity and the differential gain coefficient of the i beam polarized in k mode; Γ^k and α_{loss}^k are the confinement factor and the waveguide loss of an SOA in k mode; N is the carrier density; A_{eff} is the effective area of the waveguide; $\hbar$ is the reduced Planck constant; I is the injected current; e is the elementary charge; V is the active volume, and τ_s is the lifetime of the carriers governed by spontaneous emission and non-radiative recombination. η^k is the modified imbalance factor used to describe the asymmetry of optical transitions between the TE and TM modes when the tensile strain is built into the active layer of an SOA. If the tensile strain is not applied, then $\eta^k = 1$. Using Eq. (1), which neglects waveguide loss, and integrating both sides of Eq. (2) with respect to z yield,

#8154 - $15.00 USD Received 18 July 2005; Revised 27 September 2005; Accepted 2 October 2005

$$\frac{d\sigma}{dt} = -\frac{\sigma - \sigma_0}{\tau_s} - \sum_{i,k} \frac{\wp_{0,i}^k}{\Gamma^k \hbar \omega_i A_{eff}} \cdot \left\{ \exp\left[\Gamma^k a_i^k \left(\eta^k \sigma - N_i \ell \right) \right] - 1 \right\} \tag{3}$$

where $\sigma_0 = \tau_s I / \left(e A_{eff} \right)$ and $\wp_{z,i}^k = \wp_i^k(z)$. $\sigma = \int_0^\ell N(t,z)dz$ and ℓ are the integrated carrier density and the length of an SOA, respectively. The phase of the output converted signal is,

$$\psi_2^k = -\frac{\alpha_H}{2} \Gamma^k a_2^k \left[\eta^k \sigma - N_2 \ell \right] \tag{4}$$

where α_H is the linewidth enhancement factor.

The optical power, the integrated carrier density and the output phase associated with harmonically modulated input optical fields, can be expressed as $\wp_{z,i}^k = P_{z,i}^k + \Delta p_{z,i}^k e^{j\Omega t} + c.c$, $\sigma = \zeta + \Delta\zeta e^{j\Omega t} + c.c$ and $\psi_2^k = \phi_2^k + \Delta\phi_2^k e^{j\Omega t} + c.c$, respectively. The CW beam exhibits no input modulation and $\Delta p_{0,2}^k = 0$. Considering only the first-order terms in Eq. (3) yields the small-signal response of the integrated carrier density,

$$\Delta\zeta = \frac{-\sum_k \frac{\left(G_1^k - 1 \right)}{\Gamma^k a_1^k \eta^k P_{sat,1}^k} \Delta p_{0,1}^k}{j\Omega\tau_s + 1 + \sum_{i,k} \frac{G_i^k P_{0,i}^k}{P_{sat,i}^k}} \tag{5}$$

where $G_i^k = \exp\left[\Gamma^k a_i^k \left(\eta^k \zeta - N_i \ell \right) \right]$ and $P_{sat,i}^k = \hbar \omega_i A_{eff} / \left(\tau_s a_i^k \eta^k \right)$. Similarly, the small-signal response of the intensity and phase of the converted CW beam are,

$$\Delta p_{\ell,2}^k = G_2^k P_{0,2}^k \Gamma^k a_2^k \eta^k \Delta\zeta \tag{6}$$

$$\Delta\phi_2^k = -\frac{\alpha_H}{2} \Gamma^k a_2^k \eta^k \Delta\zeta \tag{7}$$

Notably, Eq. (6) is the small-signal response of XGM. In XPoM, the amplitude conversion is associated with interference between the TE and TM modes. Therefore, the output power of the CW beam behind a polarization controller (PC) and a polarizer, $\wp_{Pol,2}$, is given by,

$$\wp_{Pol,2} = \frac{1}{2} \left| \cos\theta \cdot \sqrt{\wp_{\ell,2}^{TE}} - \sin\theta \cdot \sqrt{\wp_{\ell,2}^{TM}} \cdot e^{j(\Phi + \Delta\Phi)} \right|^2 \tag{8}$$

where θ and Φ are the parameters that specify the polarization state, which could be adjusted by a PC. $\Delta\Phi = \Delta\phi_2^{TM} - \Delta\phi_2^{TE}$ is the relative phase difference between the TE and TM modes of the output CW beam. To maximize the extinction ratio (ER) after the polarizer, θ must be chosen to ensure that the TE and TM modes beyond the polarizer have equal DC intensity, such that $\cos^2\theta \cdot P_{\ell,2}^{TE} = \sin^2\theta \cdot P_{\ell,2}^{TM} \equiv P_\theta$ and Φ is selected to ensure that $\wp_{Pol,2}$ has a minimum zero level. For example, $\Phi + \Delta\Phi(0) = 0$ should be applied for the

#8154 - $15.00 USD Received 18 July 2005; Revised 27 September 2005; Accepted 2 October 2005

non-inverting operation, where $\Delta\Phi(0)$ is the phase difference when the input signal is logical zero. Thus, under these conditions, the small-signal response of XPoM, $\Delta p_{Pol,2}$, given by Eq. (8), could be written as,

$$\Delta p_{Pol,2} = P_\theta \sin\Phi \cdot \Delta\Phi + \frac{1}{2}(1-\cos\Phi)\left(\cos^2\theta \cdot \Delta p_{\ell,2}^{TE} + \sin^2\theta \cdot \Delta p_{\ell,2}^{TM}\right) \tag{9}$$

The first and second terms on the right-hand side of Eq. (10) are associated with XPM and XGM, respectively. Equations (5)-(7) and (9) yield,

$$\Delta p_{Pol,2} = -\frac{\left[\chi(1+r_{me})+(1-r_{me})\right]\sin\Phi}{j\Omega+\tau_s^{-1}+\tau_{stim,1}^{-1}+\tau_{stim,2}^{-1}} \times \frac{\alpha_H}{2\tau_s}\sum_k\left[\frac{\Gamma^{TE}a_2^{TE}\eta^{TE}P_\theta}{\Gamma^k a_1^k \eta^k P_{sat,1}^k}\left(G_1^k-1\right)\Delta p_{0,1}^k\right] \tag{10}$$

where $\tau_{stim,i}^{-1} \equiv \sum_k G_i^k P_{0,i}^k \big/ \left(\tau_s P_{sat,i}^k\right)$ is the lifetime of the carriers governed by the stimulated emission of the i beam; $\chi \equiv (1-\cos\Phi)/(\alpha_H \sin\Phi) = \alpha_H^{-1}\tan(\Phi/2)$ is a parameter that is related to the operating point, Φ; $r_{me} \equiv \left(\Gamma^{TM}a_2^{TM}\eta^{TM}\right)/\left(\Gamma^{TE}a_2^{TE}\eta^{TE}\right)$ represents the strength of the dependence of an SOA on the polarization, and is smaller than unity in general. In Eq. (10), the factor defined as $\xi \equiv \left[\chi(1+r_{me})+(1-r_{me})\right]\sin\Phi$ influences conversion logic and the efficiency of XPoM. Therefore, $\xi > 0$ and $\xi < 0$ represent the implementation of XPoM according to an inverted and a non-inverted conversion scheme, respectively. However, Eqs. (6) and (10) reveal that the small-signal bandwidths of XGM and XPoM are the same, and are constrained by the lifetime of the carriers.

4. Small-signal models of DXPoM

The small-signal response of DXPoM can be obtained by simply modifying Eq. (10). If the delay, Δt, is added to the TM mode, then Eq. (10) becomes,

$$\begin{aligned}\Delta p_{Pol,2} = &\left\{\frac{\left[\chi\left(1+r_{me}e^{-j\Omega\Delta t}\right)+\left(1-r_{me}e^{-j\Omega\Delta t}\right)\right]}{j\Omega+\tau_{tot}^{-1}}\right\} \\ &\times\left\{-\frac{\alpha_H\sin\Phi}{2\tau_s}\sum_k\left[\frac{\Gamma^{TE}a_2^{TE}\eta^{TE}P_\theta}{\Gamma^k a_1^k\eta^k P_{sat,1}^k}\left(G_1^k-1\right)\Delta p_{0,1}^k\right]\right\}\end{aligned} \tag{11}$$

where $\tau_{tot}^{-1} \equiv \tau_s^{-1}+\tau_{stim,1}^{-1}+\tau_{stim,2}^{-1}$. Clearly, the first bracket in Eq. (11) determines the modulation bandwidth of DXPoM. Therefore, this term divided by $(\chi+1)\tau_{tot}$ is defined as a transfer function $T(\Omega)$:

$$T(\Omega) \equiv \frac{1-\gamma e^{-j\Omega\Delta t}}{1+j\Omega\tau_{tot}} \tag{12}$$

where $\gamma = r_{me}(1-\chi)/(1+\chi)$. Equation (12) can be rewritten as a normalized transfer function to take into account explicitly the improvement in the bandwidth of DXPoM:

$$T_N(\Omega') \equiv \frac{1-\gamma e^{-j\Omega'\Delta t'}}{(1+j\Omega')(1-\gamma)} \tag{13}$$

#8154 - $15.00 USD Received 18 July 2005; Revised 27 September 2005; Accepted 2 October 2005

where $\Omega' = \Omega\tau_{tot}$ and $\Delta t' = \Delta t/\tau_{tot}$ are the normalized angular frequency and the normalized delay, respectively.

Although Eq. (13) cannot be solved analytically to yield the modulation bandwidth with arbitrary delay, the minimum and maximum bandwidths that correspond to $\Delta t' = 0$ and $\Omega'|\Delta t'| = \pi$ can be derived as,

$$\Omega'_{n,\min} = \sqrt{n^2 - 1} \tag{14}$$

$$\Omega'_{n,\max} = \sqrt{\left(n\frac{1+\gamma}{1-\gamma}\right)^2 - 1} \cong n\frac{1+\gamma}{1-\gamma} \tag{15}$$

where n is the parameter used to describe the 1/n bandwidth, Ω'_n. Equation (15) shows the improvement in bandwidth depends on γ, which is related to the operating point and the properties of an SOA. However, the minimum bandwidth represents the traditional XPoM, in which the corresponding bandwidth of Eq. (14) is independent of γ.

The γ value of an SOA determines the performance of the transfer function, so a numerical simulation is carried out to illustrate the concept of γ value. The parameters presented in Table 1 and the basic propagation equations, Eqs. (1) and (2), indicate the polarization-dependent gain (PDG) is 1.3 dB; τ_{tot} is around 30 ps and the values of γ are 0.882 and 0.852, for non-inverted and inverted conversions, respectively. Additionally, no tensile strain is applied on the SOA, so η^k are unity. Then, PDG is 8 dB, and γ are 0.724 and 0.665 for non-inverted and inverted conversions, respectively.

Table 1. Parameters Definitions and Their Values

Parameter	Symbol	Value	Units
Confinement factor	Γ^{TE}, Γ^{TM}	0.2, 0.15	
Differential gain coefficient	a_i^{TE}, a_i^{TM}	2.0×10^{-20}, 1.85×10^{-20}	m^2
Modified imbalance factor	η^{TE}, η^{TM}	0.89, 1.11	
Spontaneous carrier lifetime	τ_s	500	ps
Linewidth enhancement factor	α_H	5	
Carrier density at transparency	N_i	1.1×10^{24}	m^{-3}
Injected current	I	100	mA
Length of the SOA	ℓ	5×10^{-4}	m
Effective area of the SOA	A_{eff}	1.5×10^{-13}	m^2
Input CW power	$\wp_{0,2}$	5	dBm
Input signal power	$\wp_{0,1}$	1	dBm
Signal ER		10	dB

Figure 3 depicts the normalized 1 dB bandwidth, n =1.26, with various values of γ. As γ approaches unity, $\Omega'_{1-dB,\max}$ becomes greater and the corresponding normalized delay, $|\Delta t'|$, decreases. Moreover, the square marks in Fig. 3 clearly show that the approximation in Eq. (15) is reasonable. The bandwidth is maximized by choosing γ close to unity, indicating that r_{me} and χ must be close to one and zero, respectively. Therefore, the SOA exhibits minimum PDG. However, according to Eq. (11), this will reduce the conversion efficiency. Therefore, a trade-off exists between maximizing the bandwidth and maximizing the conversion efficiency. Furthermore, compared with a non-inverted conversion scheme, an inverted

#8154 - $15.00 USD Received 18 July 2005; Revised 27 September 2005; Accepted 2 October 2005

conversion scheme always suffers less bandwidth improvement, but has larger conversion efficiency due to the different values of γ governed by different operating points

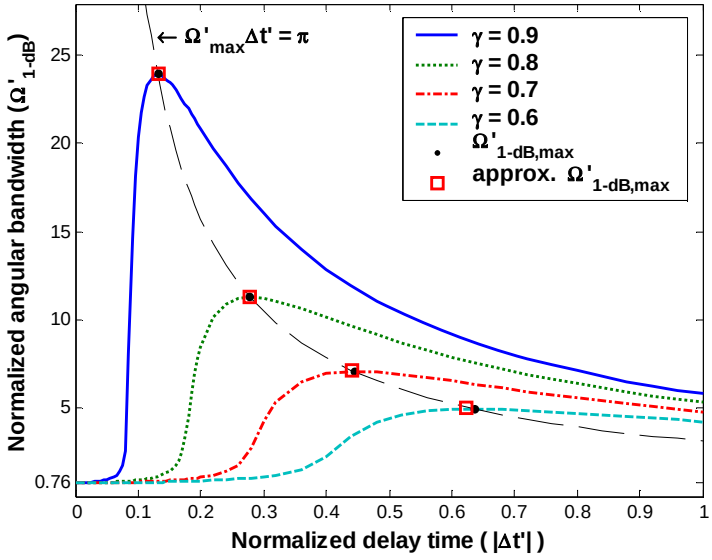

Fig. 3. Normalized 1 dB angular bandwidth of DXPoM with different values of γ.

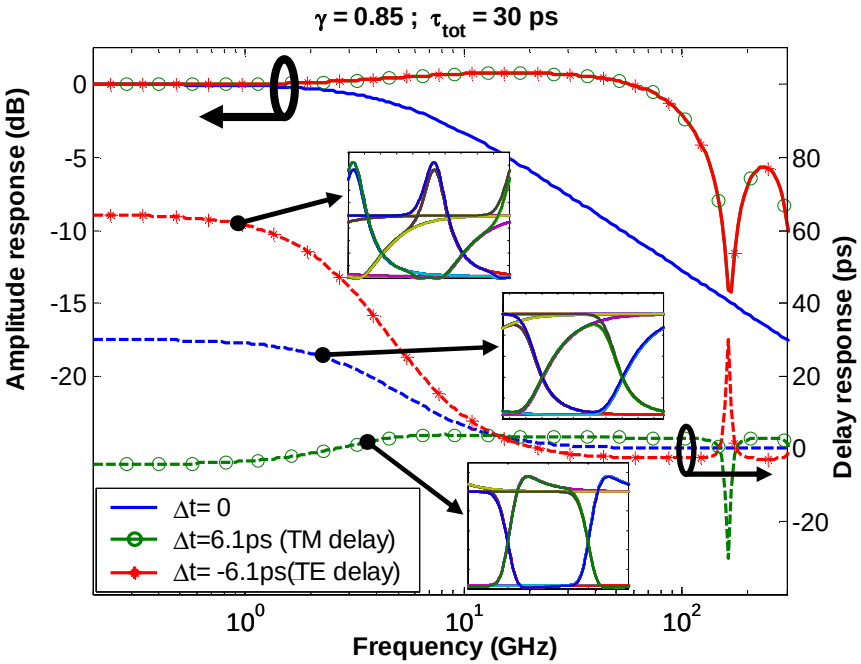

Fig. 4. Amplitude and delay responses of XPoM, DXPoM with TM delay and DXPoM with TE delay and corresponding simulated eye-diagrams

#8154 - $15.00 USD Received 18 July 2005; Revised 27 September 2005; Accepted 2 October 2005

When Δt is positive (negative), DXPoM operates with a TM (TE) delay. Figure 4 compares $T(\Omega) = |T(\Omega)| \exp(j\Theta(\Omega))$ of the TE delay with that of the TM delay, with γ = 0.85, τ_{tot} = 30 ps and $|\Delta t|$ = 6.1 ps, corresponding to a maximum 1 dB bandwidth in Eq. (15). Figure 4 demonstrates that although DXPoMs with TM and TE delay exhibit identical amplitude responses, they exhibit different delay responses, $-d\Theta/d\Omega$. The TE delay has the worst phase response which drastically distorts the converted signal. This fact explains why DXPoM with TE delay underperforms [9]. DXPoM with TM delay not only has a larger bandwidth but also a flatter delay response than XPoM. The 10 Gbps PRBS (pseudo random binary sequence) input signal spectrum is directly multiplied by the transfer functions plotted in Fig. 4 to elucidate the effects of the phase response on the signal distortion. The results after inverse Fourier transform back to the time domain are illustrated in the insets in Fig. 4. The eyes closure is clearly observed in the TE delay because of the poor phase response.

5. Optimum delay of DXPoM

Figure 4 reveals that the conversion performance is determined by not only the bandwidth of the amplitude response but also the linearity of the phase response, which corresponds to the flatness of the delay response. A natural question is how to obtain the optimum delay, $\Delta t'_{opt}$, at which DXPoM exhibits the least amplitude and the least phase distortion. This question is answered firstly by considering the relationship between $\ln|T_N(\Omega')|$ and $\Theta_N(\Omega')$, which are the real and imaginary parts of $\ln(T_N(\Omega'))$, respectively. First, $s = j\Omega'$ is set and all of the zeros of $T_N(s)$ in the complex *s* plane are found as $z_T = (\ln\gamma)/\Delta t' + j\cdot(2m\pi)/\Delta t'$, where *m* are all integrals. When $\Delta t' > 0$, all zeros are in the left half of the *s* plane and this system is a minimum phase system (MPS) [12]. An interesting characteristic of an MPS is that the amplitude and phase responses are Hilbert transforms of each other. It has been demonstrated that a constant logarithmic amplitude response implies a linear phase response, as these responses are a Hilbert transform pair [12]. Hence, only the flatness of the amplitude response of $T_N(\Omega')$ must be considered in optimizing the extra delay. Approximating $\exp(-j\Omega'\Delta t')$ in Eq. (13) as $1 - j\Omega'\Delta t' - (\Omega'\Delta t')^2/2$ and forcing $|T_N(\Omega')| = 1$, yield the optimum delay,

$$\Delta t'_{opt} = \frac{1-\gamma}{\sqrt{\gamma}} \tag{16}$$

which corresponds to simultaneous a flat amplitude response and a linear phase response. According to Eq. (15), this delay corresponds to a maximum bandwidth of $n = \pi\sqrt{\gamma}/(1+\gamma)$. Figure 5 plots the amplitude and delay responses at delays of $\Delta t'_{opt}$, $0.95\,\Delta t'_{opt}$ and $1.05\,\Delta t'_{opt}$. The dotted lines in Fig. 5 represent the second-order approximations of the amplitude responses. The good match at low frequency indicates that this approximation can be applied to determine the optimum delay. Furthermore, a nearly constant delay response and the flattest amplitude response are achieved simultaneously by applying $\Delta t'_{opt}$.

6. Time domain performance

Much information concerning the time domain can be obtained from the impulse response, which is the inverse Fourier transform of the frequency response, as well as from the frequency response, itself, of the small-signal model. The inverse Fourier transform and Eq. (13) yield the following impulse response.

(17)

#8154 - $15.00 USD Received 18 July 2005; Revised 27 September 2005; Accepted 2 October 2005

$$\mathbb{F}^{-1}\left\{\frac{T(\Omega)}{\sqrt{2\pi}}\right\} = e^{-t'}u(t') - \gamma \cdot e^{-(t'-\Delta t')}u(t'-\Delta t')$$

where $u(t')$ is a unit step function and t' is the normalized time. Figure 6 plots several impulse responses with different values of γ and $\Delta t'$. Figure 6(a) presents the impulse response of XPoM without an extra delay, and Fig. 6(b) presents that of DXPoM with the optimum TM delay, as determined by Eq. (16). Figure 6(b) clearly presents a narrower response, because the extra delay cancels the relaxation tail that is associated with a finite lifetime of the carriers. However, increasing the delay beyond the optimum value may increase the response time, as shown in Fig. 6(c). In Fig. 6(d), γ is closer to unity than in Fig. 6(b), so the response is narrower and the delay required optimizing the response time is shorter. These phenomena are consistent with the tendency in Fig. 3. Furthermore, unlike Fig. 6(b), Fig. 6(e) illustrates the case of TE delay. Although the TE delay and the TM delay are associated with the same bandwidth in Fig. 4, the impulse responses of Figs. 6(b) and 6(e) are such different due to their different phase performance. Restated, the impulse response of Fig. 6(e) is so poor that the TE delay cannot improve the conversion performance.

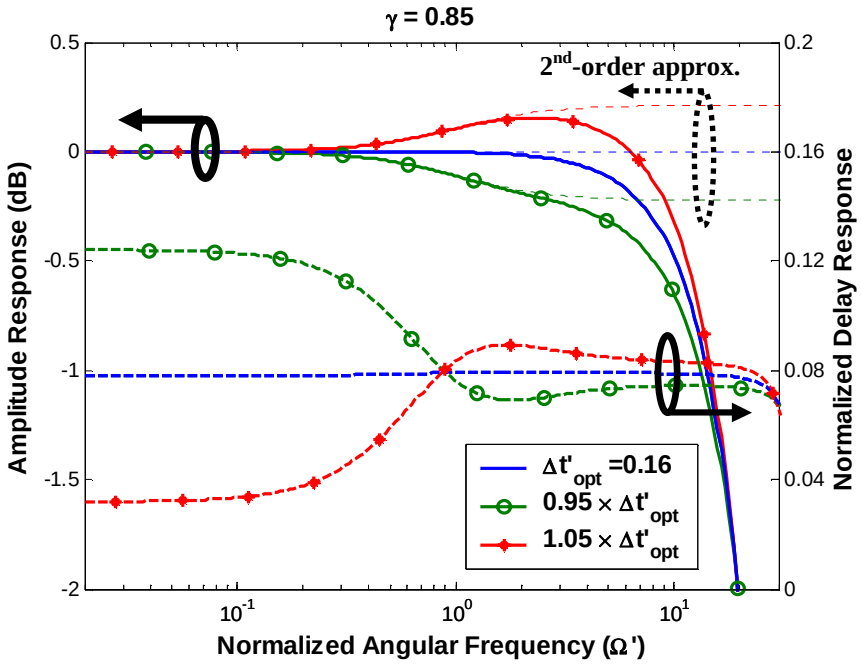

Fig. 5. Amplitude and phase responses with delay of $\Delta t'_{opt}$, $0.95\,\Delta t'_{opt}$ and $1.05\,\Delta t'_{opt}$.

7. Conclusion

This study presents small-signal models of XPoM and DXPoM for the first time. In these models, the relationships between the bandwidth improvement provided by DXPoM and several parameters are readily observed. The substantial difference between the conversion performance of TM delay and that of TE delay is explained by the phase responses of the small-signal model. The optimum delay that corresponds to both the flattest amplitude and the optimal delay responses is analytically determined. In addition to those in the frequency

#8154 - $15.00 USD Received 18 July 2005; Revised 27 September 2005; Accepted 2 October 2005

domain, the impulse responses of the DXPoM in the time domain are derived to provide further insight into the performance improvement.

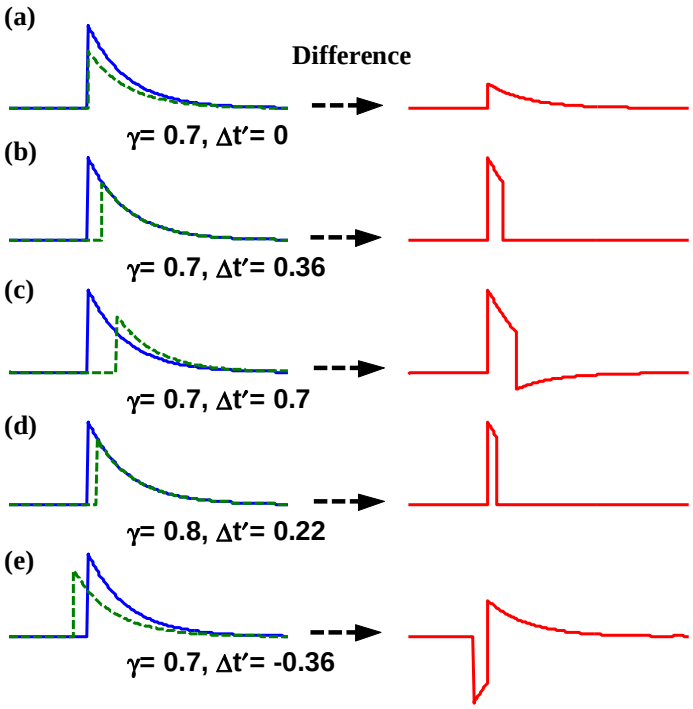

Fig. 6. Impulse responses of several conditions.

Acknowledgment

The authors would like to thank the National Science Council, Republic of China, Taiwan for financially supporting this research under Contract No. NSC 93-2215-E-009-027.